remote sensing

MDPI

Article

Tracing Magma Migration at Mt. Etna Volcano during 2006–2020, Coupling Remote Sensing of Crater Gas Emissions and Ground Measurement of Soil Gases

Salvatore Giammanco, Giuseppe Salerno *, Alessandro La Spina, Pietro Bonfanti, Tommaso Caltabiano, Salvatore Roberto Maugeri, Filippo Murè and Paolo Principato

Istituto Nazionale di Geofisica e Vulcanologia-Osservatorio Etneo, Sezione di Catania, 95125 Catania, Italy; salvatore.giammanco@ingv.it (S.G.); alessandro.laspina@ingv.it (A.L.S.); pietro.bonfanti@ingv.it (P.B.); tommaso.caltabiano@ingv.it (T.C.); roberto.maugeri@ingv.it (S.R.M.); filippo.mure@ingv.it (F.M.); paolo.principato@ingv.it (P.P.)

* Correspondence: giuseppe.salerno@ingv.it; Tel.: +39-095-7165800

Abstract: The geochemical monitoring of volcanic activity today relies largely on remote sensing, but the combination of this approach together with soil gas monitoring, using the appropriate parameters, is still not widely used. The main purpose of this study was to correlate data from crater gas emissions with flank emissions of soil gases at Mt. Etna volcano from June 2006 to December 2020. Crater SO_2 fluxes were measured from fixed stations around the volcano using the DOAS technique and applying a modeled clear-sky spectrum. The SO_2/HCl ratio in the crater plume was measured with the OP-FTIR technique from a transportable instrument, using the sun as an IR source. Soil CO_2 efflux coupled with the $^{220}Rn/^{222}Rn$ activity ratio in soil gases (named SGDI) were measured at a fixed monitoring site on the east flank of Etna. All signals acquired were subject both to spectral analysis and to filtering of the periodic signals discovered. All filtered signals revealed changes that were nicely correlated both with other geophysical signals and with volcanic eruptions during the study period. Time lags between parameters were explained in terms of different modes of magma migration and storage inside the volcano before eruptions. A comprehensive dynamic degassing model is presented that allows for a better understanding of magma dynamics in an open-conduit volcano.

Keywords: Mt. Etna; crater SO_2 flux; halogen fluxes; soil radon; soil CO_2 flux; eruptive activity; magma degassing

Citation: Giammanco, S.; Salerno, G.; La Spina, A.; Bonfanti, P.; Caltabiano, T.; Maugeri, S.R.; Murè, F.; Principato, P. Tracing Magma Migration at Mt. Etna Volcano during 2006–2020, Coupling Remote Sensing of Crater Gas Emissions and Ground Measurement of Soil Gases. *Remote Sens.* **2024**, *16*, 1122. https://doi.org/10.3390/rs16071122

Academic Editors: Zhong Lu and Jonathan Procter

Received: 16 February 2024
Revised: 12 March 2024
Accepted: 20 March 2024
Published: 22 March 2024

1. Introduction

The geochemical monitoring of volcanic gas emissions at active volcanoes has become a common and useful tool in order to understand the dynamics of magma as it approaches the surface and, therefore, to forecast eruptions [1]. In recent years, among the many techniques used for gas monitoring, those involving the remote sensing of crater gas plumes have become dominant due to the increasing sensitivity and reliability of the instruments used, their easy setup in continuous measurement mode from fixed sites and, last but not least, the greater safety for the field operators compared to other geochemical techniques [2]. The most widely used techniques for the remote sensing of crater gas emissions, especially those using solar light absorption (both in the ultraviolet and in the infrared spectra) modes of operation, concern only a few specific gas species, namely SO_2, HCl and occasionally HF. These gases, according to their pressure-dependent solubility in magma, normally escape from silicate melts at a depth shallower than 4–5 km below the surface [3–7], being extensively used as mid-term to short-term precursors of volcanic eruption [8–14]. However, for the above reasons, volcano monitoring based solely on the detection of those crater gases does not provide information on the deep-seated magmatic

processes that mark the onset of long-standing cycles of volcanic activity and thus constitute potential long-term precursors of eruptions. In this sense, recent efforts have been made to measure the crater emissions of CO_2, a gas whose release from magma starts at depth greater than 5 km below the surface [15,16], but the methods used generally imply the setup of monitoring devices near active craters, which often lead to a loss of data due to logistic problems (mostly: difficult maintenance due to extreme operational conditions and instrumental damages caused by eruptive activity).

On Mt. Etna (Figure 1), volcanic gas monitoring in the last thirty years has been carried out traditionally using remote sensing techniques (COSPEC, then UV-DOAS and FTIR) [17] and field surveys of soil CO_2 [18], the latter being recently coupled with soil ^{222}Rn and ^{220}Rn concentrations [19]. The use of radon isotopes has become increasingly common on Mt. Etna because they provide useful information on the geodynamics of an active volcanic area. In fact, in soil gases, both ^{220}Rn and ^{222}Rn originate in relatively shallow crustal rocks, and their initial amount is proportional to the concentration of parental radionuclides (^{232}Th and ^{238}U, respectively). Given the large difference in the half-lives of the two isotopes (55 s for ^{220}Rn, compared with 3.8 days for ^{222}Rn), ^{220}Rn is shallow-sourced (at most, a few tens of meters below the ground surface), whereas ^{222}Rn may come from deeper levels of the crust: up to a couple of km below the surface according to recent studies [20].

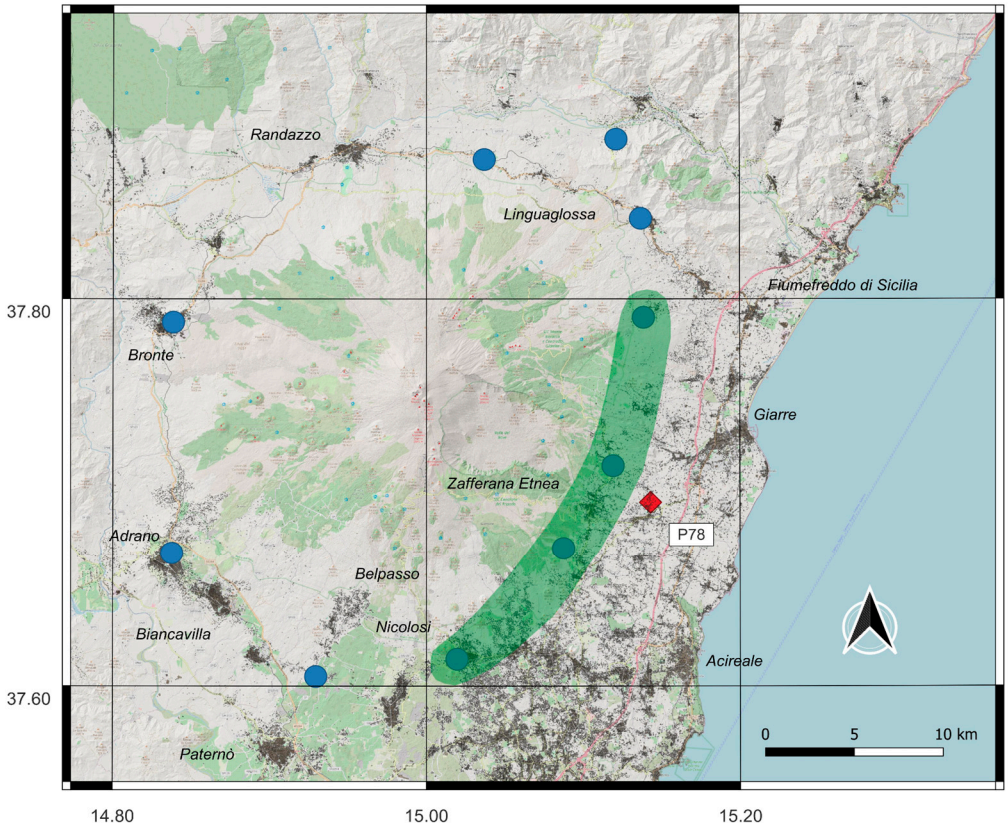

Figure 1. Schematic map of Mt. Etna with the location of the SGDI measurement site (P78) and the location of the SO_2 flux fixed monitoring stations belonging to the FLAME network set by INGV-OE (blue circles; a network of scanning ultraviolet spectrometers), the location where open-path Fourier transform infrared (OP-FTIR) spectrometry samplings were routinely carried out (green area).

Although recent studies have already investigated the combined use of crater gas emissions and soil gas emissions at Mt. Etna [21,22], this paper shows the results of the first attempt to combine data on crater SO_2 fluxes, data on crater SO_2/HCl ratios and data on soil CO_2 effluxes coupled with soil ^{222}Rn and ^{220}Rn concentrations, which were all measured over a very long period of time. The present investigation spans almost fourteen years, from June 2006 to December 2020. By using this novel approach, it was also

possible to better constrain the results of the measurements from remote sensing methods. The data acquired allowed highlighting and following long-standing cycles of volcanic activity, in particular the one including the birth, growth and end of the so-called New Southeast Crater, the newest and most active among the summit craters of Mt. Etna [23–25]. In addition, some of the strongest variations observed in all parameters were interpreted as pre-eruptive anomalies whose pattern and temporal development helped us better understand the mechanisms of magma transfer and eruption at Mt. Etna. The approach used in this investigation is, therefore, believed to be a potential new standard method for volcano monitoring.

2. Materials and Methods

Daylight measurements of bulk sulfur dioxide (SO_2) flux in the volcanic plume of Etna were performed by the FLAME (FLux Automatic MEasurement) scanning ultraviolet spectrometer network set up by INGV-OE. The network consists of nine stations spaced ~7 km apart and installed at altitudes of ~900 m a.s.l. on the volcano flanks [26,27]. Each device scans the sky on a vertical plane over 156° wide, intersecting the plume, when present, at a distance of ~14 km from the summit craters. Spectra are inverted on site applying the DOAS technique and using a modeled clear-sky spectrum [28,29]. They are then transmitted to INGV-OE where mass flux is in real time and automatically computed. Uncertainty in flux values ranges between −22% and +36% [27–29]. A detailed description of the SO_2 plume flux measurement method can be found in [26,28].

The crater gas composition in terms of bulk SO_2/HCl molar ratio was determined using an Open-Path Infrared spectrometer (OP FTIR—Fourier Transform Infrared Spectroscopy) using the sun radiation as the infrared source. The solar occultation methodology, in which the gasses plume is interposed between the sun and spectrometer [17,30], provides information on the plume contents of SO_2 and HCl, gas species with negligible concentrations in the free atmosphere that are, conversely, abundant in volcanic emissions. This technique was used during measurements carried out from different sites around the volcano, following the plume direction and according to the sun position. The collected spectra were evaluated using the FTIR_FIT software v. 1.06 [4]. This analysis package is based on a non-linear least-squares fitting algorithm and a forward model in order to calculate radiative transfer in a two-layer model atmosphere (one for hot volcanic gas and another for ambient temperature atmospheric gasses [30]). The analytical error on concentrations was less than 4%. Molar ratios were determined by measuring 100 or more spectra per each measurement sequence and then by plotting the retrieved amounts of SO_2 against those of HCl. The gradient of linear regression plots provides the SO_2/HCl ratio.

Soil CO_2 effluxes were measured on site using the accumulation chamber method [31–33]. This method consists of measuring the rate of increase in the CO_2 concentration inside a cylindrical chamber, with an open bottom, placed on the ground surface and connected with a portable NDIR (nondispersive infrared) spectrophotometer (PP Systems, Amesbury, MA, USA, mod. EGM4). An internal fan in the chamber allows for an efficient gas mixing. The increase in concentration during the initial measurement is proportional to the efflux of CO_2 [32]. This is an absolute method that does not require corrections linked to the physical characteristics of the soil. Both the accuracy and the reproducibility of this method were tested in the laboratory (more details in [19]). The average error was about ± 5%, and the reproducibility in the range 200–1600 g m^{-2} d^{-1} was ± 5%.

Combined measurements of soil ^{220}Rn and ^{222}Rn were carried out on site using a portable radon meter (Durridge Company Inc., Billerica, MA, USA, mod. RAD7), which was provided with a passive ion-implanted planar silicon detector. Gas was sampled into a fixed metal probe at 40 cm depth in the soil and introduced into the RAD7 with an internal pump. Active filters preclude all other major gases and metals except CO_2. The detector chamber is energy dispersive and thus discriminates between ^{220}Rn and ^{222}Rn in the gas phase that enters it. Therefore, both ^{220}Rn and ^{222}Rn are detected by counting the alpha particles that are released from decay of their respective daughter nuclides ^{218}Po

($t^{1/2}$ = 3.05 min) and ^{216}Po ($t^{1/2}$ = 0.145 sec). In order to achieve radioactive equilibrium between ^{222}Rn and the measured daughter, ^{218}Po, each measurement takes >15 min. Furthermore, to account for the effect of CO_2 on the determination of the (^{220}Rn/^{222}Rn) activities ratio, all (^{220}Rn/^{222}Rn) values were corrected by multiplying the measured (^{220}Rn/^{222}Rn) times 1.016 for every percentage point of CO_2 above zero [34].

Based on the empirical relationship found by [19], we calculate the ratio between (^{220}Rn/^{222}Rn) and CO_2 efflux at each sampling site for each survey using the following:

$$SGDI = \varphi CO_2 / (^{220}Rn/^{222}Rn) \quad (1)$$

where SGDI is the Soil Gas Disequilibrium Index [19], φCO_2 is the soil CO_2 efflux in g m^{-2} d^{-1}, and (^{220}Rn/^{222}Rn) is the ratio of the activities of the two radon isotopes (a dimensionless number). The units of the SGDI are dimensionless, as this parameter is obtained by dividing a quantity that has units by a dimensionless quantity.

As shown by [19], the SGDI is a reliable measure of the mechanism of soil gas transport toward the surface, as it basically allows to quantify and evaluate, in both space and time, the relative contributions of environmental and volcanic/hydrothermal signals in soil gas emissions and hence to reveal anomalous changes related with gas overpressures within the volcano caused by new magma arrival and accumulation into Mt. Etna's shallow feeder system. As a general rule, low SGDI values due to a higher ^{220}Rn content indicate a shallow origin of the soil gas mixture and/or low CO_2 effluxes (with CO_2 likely being non-magmatic). Conversely, higher SGDI values due to higher ^{222}Rn contents indicate that the gas mixture comes from deeper layers of the crust, and it is normally associated with high CO_2 effluxes, which is likely due to magmatic degassing. The physical process behind this behavior is that CO_2 flowing through the crust is able to extract both ^{220}Rn and ^{222}Rn from the rocks and to carry them to the surface, but if the CO_2 efflux is high enough, as is the case of strong gas pressures at a depth caused by magmatic degassing within an active volcano, the deep ^{222}Rn can quickly reach the surface before it significantly decays out, thus lowering the ^{220}Rn/^{222}Rn ratio.

Measurements of SGDI at Mt. Etna were carried out in a site (P78 in Figure 1) that was extensively studied during the last 20 years because of its high CO_2 emissions from the soil, whose intensity is sometimes comparable to that measured at the summit fumaroles of the volcano. The origin of soil CO_2 from this site is mainly magmatic, as revealed both by the carbon isotopes composition and by the concurrent emission of other magmatic gases [35,36]. The gas at P78 is being derived mainly from the main feeder system of Etna and occasionally also from magma bodies temporarily stored at depth (between ~4 and ~10 km below the surface) into the volcano [35,36]. Recent geochemical studies, also coupled with near surface geophysics (Automatic Resistivity System and Very Low Frequencies method), in the area around P78 recognized this site as being located on a major WNW-ESE-trending fault characterized by clear anomalies in soil degassing and soil resistivity [18,37] with temporal changes in CO_2 emission linked to changes in volcanic activity [18].

3. Results

The basic statistical information on all parameters measured is summarized in Table 1. Figure 2 shows the values of each parameter plotted in time from 1 January 2006 to 31 December 2020. Crater SO_2 fluxes are shown as daily average values of the many measurements taken in a single day and are expressed in t/d. The SO_2/HCl ratios are averages of hundreds of spectra collected during each measurement session, which were carried out only under favorable weather conditions. SGDI values are those calculated from Equation (1) above in the days when measurements were carried out and are expressed in dimensionless units, as they are the result of ratios. In order to properly interpret all the data (SO_2 flux, SO_2/HCl and SGDI) and make them comparable, some statistical analyses, interpolation and filtering were necessary. In particular, shallower degassing processes are generally more sensitive to environmental conditions (including meteorological factors, the

presence of groundwater, tidal effects, etc.) than deep processes and hence the need to filter out all possible non-volcanic influences from the acquired signals.

Table 1. Values of daily averages of crater SO_2 flux (in t/d) measured from the FLAME monitoring network of INGV-OE at Mt. Etna, of SO_2/HCl ratio (in dimensionless units) measured periodically with the FTIR technique and of SGDI (in dimensionless units) measured at site P78 during the study period.

	SO_2 Flux (t/d)	**SO_2/HCl (Molar Ratio)**	**SGDI (d.u.)**
Min	172.7	1.5	1.2
Max	20,528.1	7.4	96,419.4
Mean	2700.8	3.1	5706.0
Stand. Dev.	1714.0	1.0	12,221.7
Median	2333.7	2.8	1256.4
Skewness	2.2	0.8	4.4

3.1. SO_2 Fluxes

The values of crater SO_2 flux acquired ranged from 172.7 to 20,528.1 t/d (Figure 2a). This is quite a large interval of variation, indicating a very dynamic volcanic system with many periods of replenishment of fresh magma into relatively shallow portions of the volcano feeding system. In order to investigate possible cyclic variations on SO_2 flux, we used the Fourier transform on the SO_2 temporal data, which allowed us to decompose the raw signal into oscillatory components. Before doing this, the available SO_2 flux data were interpolated in order to obtain a continuous set of values with no missing days of measurements. We performed the interpolation using a cubic-spline function and a daily sampling step (for a total of 5327 days). We used the Matlab© software package (The MathWorks Inc., version 23.2.0 (R2023b), Natick, MA, USA) to perform both this process and all following analyses. The spectrogram obtained from decomposition of the interpolated time series (Figure 3a) reveals predominant cycles corresponding to periods of about 467 days, 333 days (the strongest one in terms of spectral amplitude), 275 days, 156 days, 68 days, 45 days, 41 days, 29 days, 20 days, 18 days and minor cycles of about 1167 days, 212 days and 32 days. All of the above cycles are indicated with numbered squares (#1 to #13, in order of increasing frequency) in the spectrogram of Figure 3a.

In order to filter out the above-described cyclic component from the SO_2 flux signal, we used iteratively band-stop filters on the interpolated signal with frequency thresholds of filters set at values of frequency (in cycles/day) both immediately higher and immediately lower than those of the major frequency peaks identified above (in this case, from peak #1 to #6 in Figure 3a). Following this procedure, after inverse-transformation of the filtered signal from the frequency domain into the time domain, the new time series of SO_2 flux data was devoid of all major periodic components (Figure 4d), and therefore its variations likely reflected only (or mainly) the influence of aperiodic magmatic processes on crater degassing. However, at least two of the peaks highlighted in the periodogram of Figure 3a appeared to have a period longer than a year (peaks #1 and #2 actually correspond to 1167 and to 467 days, respectively), and they are not clearly attributable to environmental parameters. Therefore, in order to better investigate this behavior, we applied a low-pass filter on the data series (merely, a moving average of the interpolated daily data) with a higher threshold set at about one year (thus entailing all SO_2 fluctuations with a period longer than 366 days). The resulting filtered signal (Figure 5d) shows interesting long-term trends in SO_2 flux values that could be related to long-term magmatic processes occurring inside the volcanic system, and that in our opinion deserve attention and further discussion (see Section 4 below). In particular, three periods of particularly strong crater degassing were observed in early 2007, during most of 2014 and, more evidently, from late 2016 to early 2020.

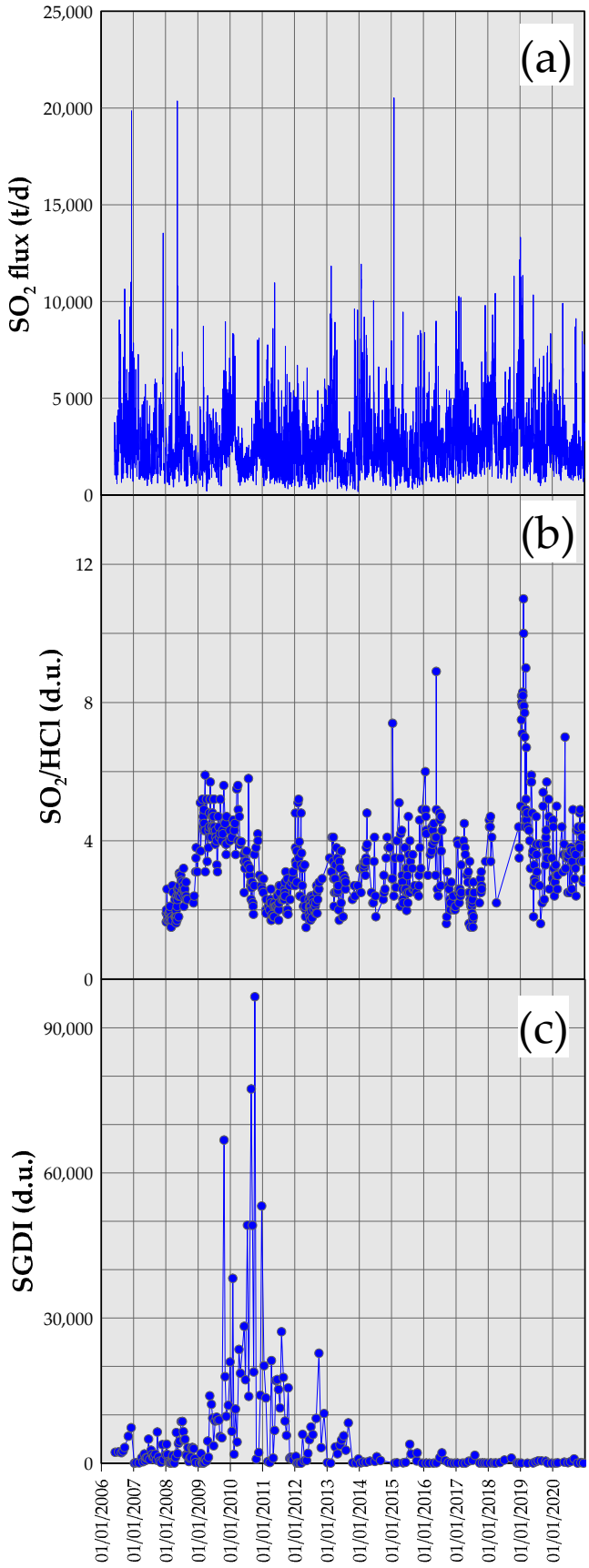

Figure 2. Temporal patterns of gas emissions (raw data) from Mt. Etna from 1 January 2006 to 31 December 2020: (**a**) Daily averages of crater SO_2 flux (t/d); (**b**) SO_2/HCl ratio in the crater plume (dimensionless units); (**c**) SGDI values (dimensionless units).

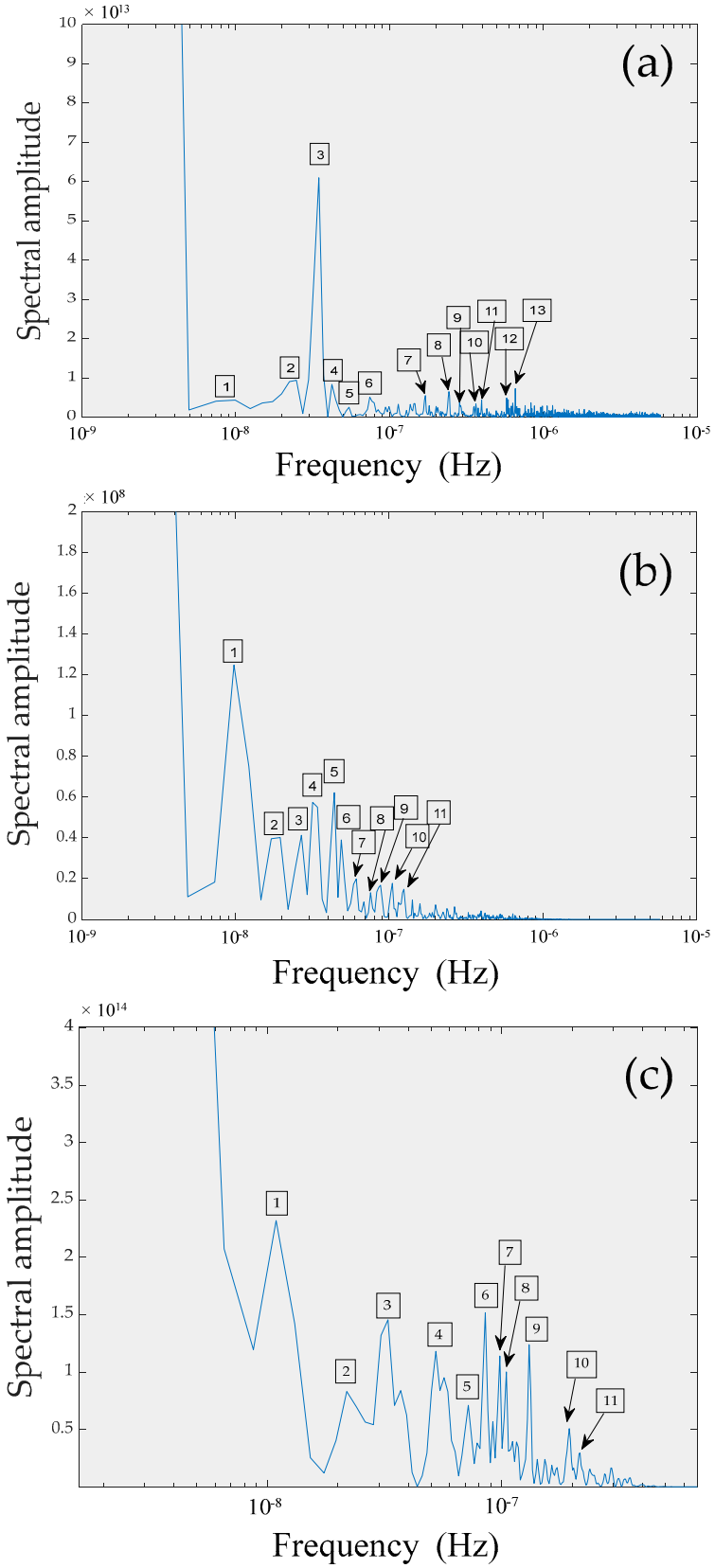

Figure 3. Spectrograms of (**a**) interpolated daily averages of crater SO_2 flux; (**b**) interpolated SO_2/HCl ratios in the crater plume; and (**c**) SGDI values. The main cycles in the frequency domains are highlighted with numbered squares (see text for details).

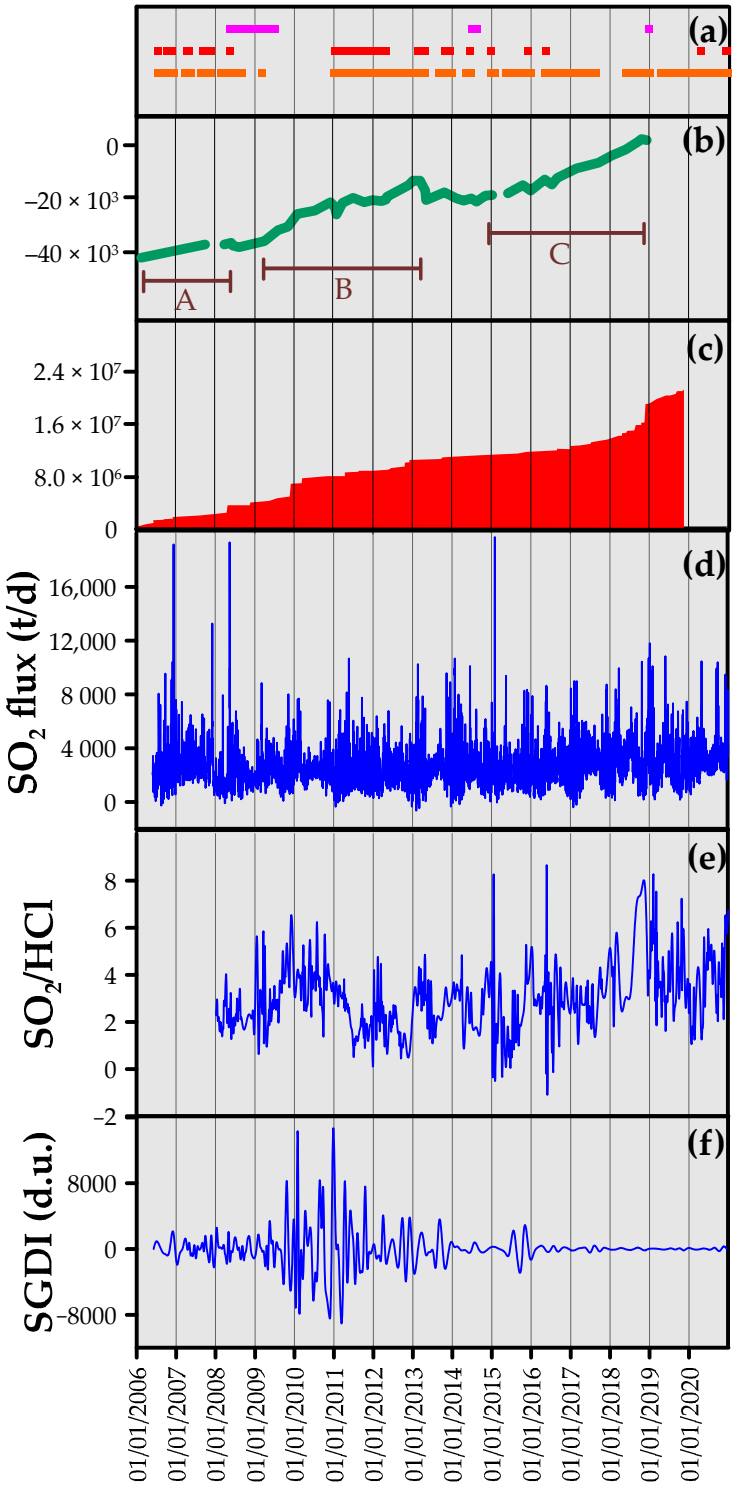

Figure 4. Temporal patterns of band-stop filtered data (i.e., after removing the main periodic signal oscillations) of gas emissions from Mt. Etna from 1 January 2006 to 31 December 2020, correlated with other relevant volcanological, geophysical and seismic parameters: (**a**) eruptive activity of Mt. Etna during the studied period, divided by type: flank eruptions (magenta symbols); paroxysms with lava fountains (red symbols); summit eruptions with strombolian activity and/or lava effusions (orange symbols); (**b**) areal dilatation data (in ppm) acquired from the EDM (Electro-optical Distance Measurement) network on the western flank of Mt. Etna until 2007, combined with dilatation data from the CGPS (Continuous Global Positioning System) EMEG-EMGL baseline on the same flank of the volcano from 2007 to 2018 (redrawn from [38]), where period A marks the inflation linked to

magma accumulation before and during the 2008–2009 flank eruption, period B marks the inflation linked to magma arrival before and during the 2011–2015 eruptions of NSEC and VOR, and period C marks the inflation that preceded the 24–27 December 2018 flank eruption and associated seismic phenomena; (**c**) cumulative seismic strain release (in $J^1/_2$) occurred at Mt. Etna from 2006 to 2019 (redrawn from [39]); (**d**) filtered crater SO_2 flux values (t/d); (**e**) filtered SO_2/HCl ratios in the crater plume (dimensionless units); (**f**) filtered SGDI values (dimensionless units).

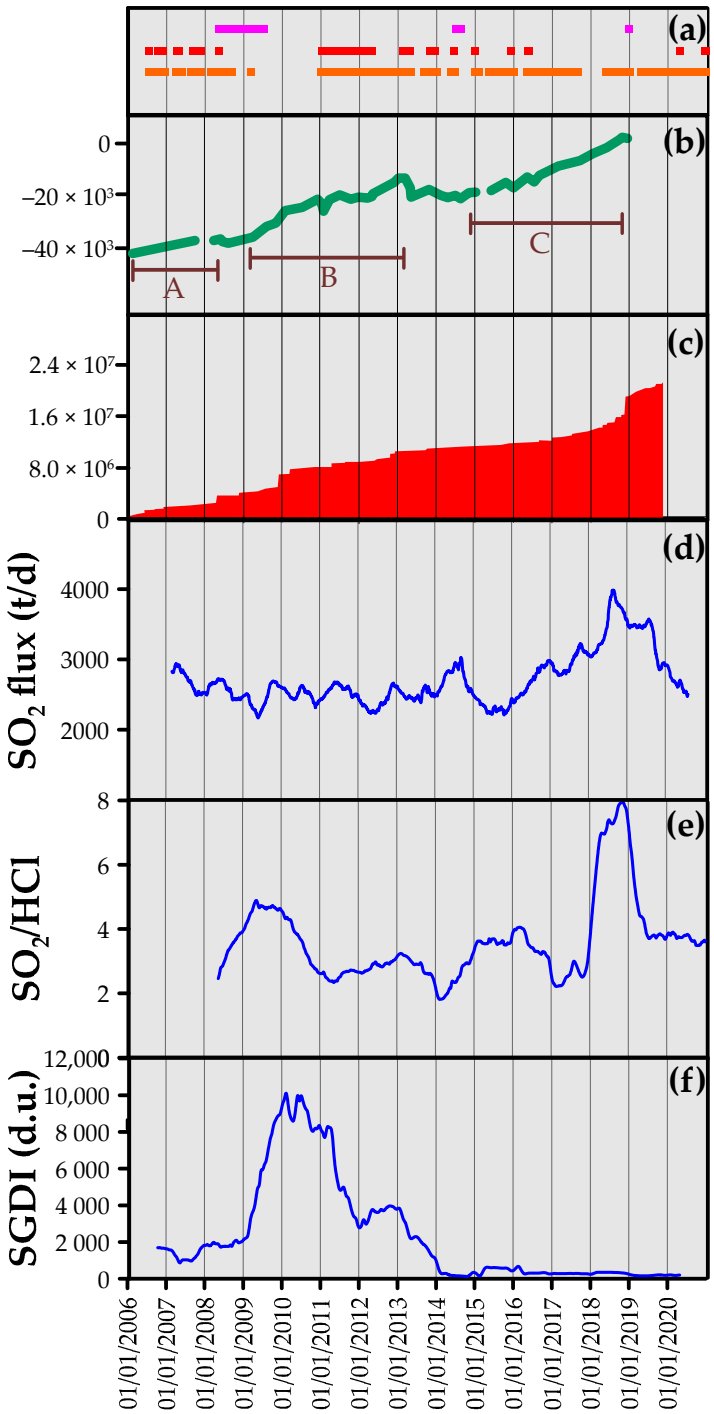

Figure 5. Temporal patterns of low-pass filtered data (after calculating centered 366-day moving averages) of gas emissions from Mt. Etna from 1 January 2006 to 31 December 2020, correlated with other relevant volcanological, geophysical and seismic parameters: (**a**) eruptive activity of Mt. Etna during the studied period, divided by type: flank eruptions (magenta symbols); paroxysms with lava fountains (red symbols); summit eruptions with strombolian activity and/or lava effusions (orange symbols); (**b**) areal dilatation

data (in ppm) acquired from the EDM (Electro-optical Distance Measurement) network on the western flank of Mt. Etna until 2007, combined with dilatation data from the CGPS (Continuous Global Positioning System) EMEG-EMGL baseline on the same flank of the volcano from 2007 to 2018 (redrawn from [38]), where period A marks the inflation linked to magma accumulation before and during the 2008–2009 flank eruption, period B marks the inflation linked to magma arrival before and during the 2011–2015 eruptions of NSEC and VOR, and period C marks the inflation that preceded the 24–27 December 2018 flank eruption and associated seismic phenomena; (**c**) cumulative seismic strain release (in $J^1/_2$) occurred at Mt. Etna from 2006 to 2019 (redrawn from [39]); (**d**) filtered crater SO_2 flux values (t/d); (**e**) filtered SO_2/HCl ratios in the crater plume (dimensionless units); (**f**) filtered SGDI values (dimensionless units).

3.2. SO_2/HCl Ratio

The data of plume SO_2/HCl ratio were acquired starting from 7 January 2008, and they were treated similarly to those of crater SO_2 flux. Values of SO_2/HCl ratio were first interpolated using a cubic-spline function and a daily sampling step (for a total of 4743 days) and then decomposed into oscillatory components with the Fourier transform. The corresponding spectrogram is shown in Figure 3b, and it highlights predominant frequency peaks corresponding to periods of about 1186 days, 677–593 days, 432 days, 312 days, 263 days, 237 days and minor ones of about 190 days, 153 days, 135 days, 110 days and 93 days. The above cycles are indicated with numbered squares (#1 to #11) in the spectrogram of Figure 3b.

As for the SO_2 flux data, those of the SO_2/HCl ratio were filtered in order to reveal the signal changes only due to magmatic processes. We therefore applied band-stop filters in the same manner as for the SO_2 flux filtering procedure, this time filtering out all of the frequency peaks highlighted in Figure 3b, and then re-transforming the filtered signal into a time-series of filtered data (Figure 4e). Also in the case of the SO_2/HCl ratio, we applied a low-pass filter to highlight long-period trends that could help understanding the long-term degassing processes that occurred during the investigated period. In particular, very high values of the SO_2/HCl ratio were observed from 2008 to 2010, in 2015–2016 and then, much more evidently, in 2018 until early 2019 (Figure 5e).

3.3. SGDI Values

During the studied period, soil (^{222}Rn) concentrations ranged from 97 to 38,850 Bq m^{-3}, soil (^{220}Rn) concentrations ranged from 97 to 6855 Bq m^{-3}, and soil CO_2 efflux values ranged from 4.44 to 4605.60 g m^{-2} d^{-1}. The corresponding calculated SGDI values ranged from 1.21 to 96,419.40 (Figure 2c). The large temporal variations observed in this parameter can be a function of either environmental or of volcanic causes, more likely a combination of both, which we attempted to identify and discriminate. Meteorological parameters, such as rainfall, air temperature and barometric pressure, can influence the soil degassing rates of CO_2 and radon isotopes, especially when those are low [18,40–48]. Both soil and fumarolic gases of Mt. Etna, actually, normally show an appreciable, if not a prevailing, air contamination (e.g., [35] and literature therein cited). Other cyclic (seasonal) parameters, such as lunar tides (Lunar Month, Lunisolar Fortnight), can influence soil degassing as well [49,50]. To test whether environmental/seasonal factors contribute to temporal changes in soil degassing, we performed a Fourier transform on the SGDI temporal data, which allowed us to decompose the raw SGDI signal into oscillatory components and thence to highlight eventual cyclic variations. Before doing this, as for the SO_2 flux and S/Cl ratio signals, discrete SGDI data were interpolated in order to obtain a continuous set of values. The interpolation was performed using a cubic-spline function and a daily sampling step (for a total of 5327 days in the case of site P78). The spectrogram obtained from decomposition of the interpolated time series (Figure 3c) reveals predominant cycles corresponding to periods of about 1060 days, 530 days, 360 days, 220 days, 136 days, 118 days, 110 days, and 88 days and minor cycles of about 160 days, 60 days and 54 days. All of the above cycles are indicated with numbered squares (1 to 11) in the spectrogram

of Figure 3c. Cycles of about 360 days and their multiples (e.g., 1060 days) are clearly related to seasonal variations with a yearly period, which were likely produced by air temperature cycles and/or the yearly component of the Earth tide [40–48,51]. Cycles of about 160–200 days are related to half-yearly periodic variations which are likely produced by rainfall during the spring and fall [52,53], and those of about 100–120 days suggest variations with a period between four-monthly and quarterly, which are possibly due to higher-frequency harmonics of the above cyclic parameter. Lastly, lunar tidal effects could explain the majority of the cyclic variations with a period of about 60 days. We again used iteratively band-stop filters on the interpolated SGDI signal. Following this procedure, after inverse-transformation of the filtered signal from the frequency domain into the time domain, the new time series of SGDI data was devoid of all major periodic components (Figure 4f), and therefore its variations likely reflected only (or mainly) the influence of aperiodic volcanic sources on soil degassing.

The effectiveness of our above filtering procedure for removing environmental influences on the SGDI time series was already tested in a previous study on the use of the SGDI in volcano monitoring [19], and a similar approach was successfully used for the filtering of near-continuous soil gas radon signals alone [54]. It must be underlined that because of the relatively low frequency in the periodic acquisition of field data, only volcanic-related processes with temporal evolution equal to or longer than the period between measurements can be observed and hence described, whilst geodynamic processes with shorter periods are likely to be missed.

The filtered daily SGDI signal (Figure 4f) showed many aperiodic oscillations, often with spike-like behavior, around the mean of the whole time series (i.e., 5.5, with standard deviation of 2121.3). Based on the intensity of these oscillations, the filtered SGDI time series can be apparently divided into three distinct periods. From the beginning of observations until 31 August 2009, the signal showed moderate oscillations that for most of the period remained roughly within the ± 1 standard deviation values, although being often close to these values and sometimes even outside them. From 1 September 2009 until 31 December 2013, the signal showed much stronger variations that very often reached values well outside the ± 1 standard deviation of mean. Lastly, from 1 January 2014 until the end of observations, the signal was very stable with no significant variations around the mean value except for the short-lived sequence of spikes observed between 4 July 2015 and 16 January 2016.

A low-pass filter applied to the original SGDI signal highlighted long-period trends, nicely corresponding to those highlighted with the previous band-stop filtering procedure, except for the SO_2 flux (Figure 5f). From 2006 to late 2009, SGDI values were unstable but relatively low. From early 2009 to 2013, values were much higher with a bell-shaped pattern peaking in the first half of 2010. Lastly, a new minor anomaly appeared in late 2015 until early 2016. Afterwards, values dropped to stable and very low levels until the end of the present investigation.

4. Discussion

Each of the three geochemical parameters considered in this study carries information on different pressure conditions (which translates into different depth) of ascending magma batches during the main exsolution phases of gases and/or on pressure conditions within the volcanic system during magma accumulation before its eruption at the surface.

Mathematical filtering of our geochemical time signals proved very useful in highlighting temporal patterns that are likely to reflect solely the dynamics of magma in terms both of its ascent velocity and of its temporary stagnation/storage inside the volcano. In particular, the band-stop filters revealed high-frequency variations without any particular trend in the SO_2 flux signal (Figure 4c). The amplitude of these changes was highly variable, and it was probably related with aperiodic convective-driven variations in the magma (at least in its uppermost part) at depth shallower than 5 km below the surface. The largest of those fluctuations were often correlated with summit paroxysmal eruptions. Conversely,

the low-pass filter on the same signal (Figure 5c) highlighted significant high values about a year before the onset of the 2008–2009 flank eruption as well as just before and during that of 2014. Furthermore, a clear multi-year increasing trend was revealed in the period 2016–2019. In particular, an evident increase in SO_2 emissions was observed since 2016, which culminated just before the 24 December 2018 flank eruption. A steady decrease was instead observed afterwards, which was more evident after the summer of 2019. This long-term trend, therefore, seems to describe the arrival of new gas-rich magma that eventually produced the short-lived "Christmas 2018" flank eruption. According to the following data on gas emissions, which remained high for many months, a significant volume of magma did not erupt on that occasion, but it resided at relatively shallow depth inside the volcano losing volatiles in excess. Actually, in the months preceding the December 2018 eruption, the volcano was characterized both by a strong increase in deep seismicity and by a marked general inflation [38,39,55]. Analysis of ground deformation data indicated two different dykes intruding into the volcano: a shallow one eventually feeding the eruption and a deeper one that was not immediately erupted and resided inside the deep structure of the volcano for years [55]. This latter is likely to have fed the long sequence of paroxysmal eruptions of 2020–2022. The increase in the SO_2 flux since 2017, observed thanks to the low-pass filtering, seems to be well explained by the evolution of a progressively shallower intrusion of magma that led to the December 2018 flank eruption. Interestingly, no clear variations in the SO_2 flux were observed during the formation of the NSEC (6 November 2009) and its subsequent growth started in 2011. In addition, no correlation was found between the SO_2 flux data and the geophysical/seismological signals associated with the early NSEC activity (Figures 4 and 5). The reason for this may be that the magma accumulated during that period was located very deep into the volcano, probably some 4 to 5 km below sea level (7 to 8 km below Etna's summit); thus, it was much deeper than the level of exsolution of SO_2 from the magma. This hypothesis is strongly supported by field data collected on 20 November 2009 by active FTIR measurements carried out on the rim of the newly opened pit of the NSEC, which showed an emitted gas phase strongly enriched in CO_2 compared to SO_2 (CO_2/SO_2 molar ratio $\cong$ 9; [56]). Furthermore, the sources of inflation retrieved during the same period from ground deformation data were located at similar depth, according to [38]. As a consequence, occasional sustained releases of SO_2 from the deep magma, therefore, occurred only during the short-lived paroxysmal episodes from January 2011 to December 2013, thus reflecting fast transfer of discrete small batches of magma directly from its deep storage volume to the surface.

The bulk SO_2/HCl molar ratio in general showed high values some months before the occurrence of the highest values of SO_2 flux (particularly in 2018). This is an indication of a lesser rate of rejuvenation of magma in the shallow portion of the plumbing system, as observed during the 2008–2009 flank eruption [17]. The latency between the two parameters is particularly evident from the low-pass filtered signals (Figure 5d,e). In detail, the band-stop filtered signal of this ratio (Figure 4e) highlighted short-lived periods with high values (that means deeper-seated gas sources) in the period 2009–2010 before the opening of the NSEC. Afterwards, high values occurred again at the very beginning or just before each sequence of lava fountains and/or strombolian eruptions in the years 2011, 2012, 2013 and 2014. Each period of higher values was then followed by a period of very low values (that means shallower-seated gas sources), corresponding with the occurrence of the above eruptive sequences and hence indicating emission of HCl from very shallow magma batches. Since the last months of 2015, however, the SO_2/HCl ratios were on average higher than before. This tendency was much more evident since the end of 2017, which marked the onset of a long period of very high values in the second half of 2018 and during most of 2019. After a return to lower values, this ratio showed a new increasing trend toward the end of 2020. As for the SO_2 flux, the SO_2/HCl ratio was moderately higher during the two sequences of strong paroxysmal events that occurred at the Central Crater in December 2015 and in May 2016. The longer-lived increase observed just before the December 2018 flank eruption indicated the arrival of relatively large amounts of magma from deeper

portions of Etna's feeding system. Differently from the SO_2 flux signal, low-pass filtering of SO_2/HCl ratios (Figure 5e) showed more or less the same results as the band-stop filtering of the same signal, just enhancing the long-term trends. In fact, four long periods of higher values were clearly observed: (i) during the 2008–2009 flank eruption; (ii) during the paroxysmal sequences of 2011–2013; (iii) before the sequence of summit eruptions of 2015–2017 and (iv) before the December 2018 eruption. Conversely, periods of markedly low values were observed during or right after each of the above periods. The alternation of high and low ratio values, in this exact sequence, would nicely reflect the progressive upward migration of deep magma batches, each one releasing the deeper gas (i.e., SO_2) first and then the shallow gas (i.e., HCl) when moving close to the surface, just before or during their eruption. This could be explained taking into consideration the different nature of SO_2/HCl and SO_2 flux signals: evidently, when the flux of SO_2 from the craters was stable and the SO_2/HCl ratio decreased, it indicated a higher proportion of HCl relative to SO_2, according to a more efficient mechanism of degassing in the shallow portion of the plumbing system of the volcano [17].

As regards the SGDI values, both types of filtered SGDI signal (Figures 4e and 5e) showed the largest anomalies between 2009 and 2014 and only a very minor one in the second half of 2015. In detail, the band-stop filtered SGDI values showed large fluctuations of the signal during the period 2009–2014. The highest peaks were observed in late 2009, then in the second half of 2010 and lastly in early 2011. Other significant peaks were observed in late 2011, late 2012 and late 2013. A minor anomaly was then observed in late 2015 and early 2016. All of the above anomalous changes until 2013 seem to have preceded the opening of the NSEC and the main phases of its paroxysmal activity, until 2014. The anomalies in 2015 seem to have preceded the sequence of paroxysmal eruptions at the Central Crater in late 2015 (and possibly also those of mid-2016). Lastly, it is worth noting that the amplitude of background SGDI signal oscillation before 2009 was markedly larger than that after 2015. This seems associated with the activity of the late SEC, which ended in May 2008, and with the 2008–2009 flank eruption. Similar indications can be obtained from the low-pass filtered SGDI signal (Figure 5e). The highest values were observed, again, between 2009 and 2013. Two main periods of high values were highlighted: the most intense one from 2009 to 2011 and a lesser one from 2012 to 2013. Only a very small further anomaly was then observed in 2015. Once again, the background values before 2009 were significantly higher than those after 2013, likely due to the input of gas from a relatively deeper source of magma, whose degassing occurred on a large scale both through the main conduits of the volcano and through faults on its flanks. Similar behaviors were already observed at Mt. Etna several times in the past few decades [18,21,57]. Because this parameter is a proxy of pressure increases and fluctuations in the feeder system of Mt. Etna [19], its variations seem to mark magma arrival and release during the final stages of eruptive activity at the SEC and then the pressure build-up associated with the formation of a new magma reservoir that eventually fed the activity of the NSEC until 2014. The subsequent release of pressure in this new reservoir since 2011 is explained with its progressive emptying due to the start of the long sequence of paroxysmal eruptions at the NSEC that ended in December 2013. A new, though less intense, moment of pressure build-up occurred in late 2012, during a pause in the eruptions at the NSEC. After 2013, only mild sub-terminal effusive eruptions occurred in 2014. These latter seemingly completed the emptying of the NSEC reservoir, which later was no longer pervaded by magma. According to the above interpretation of the SGDI signal, the eruptive activity at Etna after 2014 was fed by magma that either did not reside into the shallowest portion of the volcano feeder system for so long or whose volume was not so large as to produce marked soil gas anomalies at the surface. In this sense, the weak anomaly from early 2015 to early 2016 is a partial exception.

In large part, the above interpretations of the geochemical data are confirmed by comparison between all filtered gas signals and other signals obtained from the INGV-OE monitoring network. In particular, we considered: (a) volcanological data on the eruptive events that occurred during the studied period, divided into flank eruptions (i.e., those occurring from well-developed eruptive fissures located at lower elevation than the summit craters and independently fed), paroxysmal summit eruptions (short-lived, with lava fountains and often lava flow emission directly spilling over the summit craters or emitted from fissures opening on the flanks of the summit cones) and milder summit eruptions (long-standing, often and gentle lava effusion from fissures generally opening at the foot of the summit cones); (b) areal dilatation data acquired from the EDM (Electro-optical Distance Measurement) network on the western flank of Mt. Etna until 2007, later combined with dilatation data from the CGPS (Continuous Global Positioning System) EMEG-EMGL baseline on the same flank of the volcano from 2007 to 2018 [38]; (c) cumulative seismic strain release from earthquakes that occurred in the volcano area [39]. In general, the largest anomalies in our filtered degassing signals, both considering the band-stop filtered and the low-pass filtered data, were well correlated with periods of increased seismicity and ground deformation and were followed by increased eruptive activity, mostly in terms of summit or flank eruptions (Figure 4 and 5). The correlations found among all signals considered, both geochemical and geophysical, helped us develop a comprehensive dynamic degassing model of Mt. Etna during the monitored period, as described in the next section.

5. Degassing Model

The main points that arise from the correlation between all signals considered are listed below and are graphically condensed in the dynamic model of Figure 6:

(a) The situation before 2009 is compatible with the emptying of a shallow magma reservoir that was feeding the 2008–2009 flank eruption. Emptying of this reservoir caused the high SO_2/HCl and moderate crater SO_2 flux with no significant flank degassing because magma was already depleted in the deep gases;
(b) The situation during the period 2009–2014 indicated the formation of a deep (about 4–5 km bsl) magma reservoir that eventually fed the activity of the newborn NSEC. This led to marked flank degassing of deep origin and moderate plume bulk degassing.
(c) The situation from about 2015 to 2020 suggested magma migration to shallow levels (1–2 km bsl) of the volcano plumbing system with sustained crater plume bulk degassing and negligible flank emissions of soil gases. This period culminated with the 2018 flank eruption.

According to the above model, the end of the sequence of paroxysmal eruption at NSEC in 2013 and the beginning of the long-standing and slow effusions of lava flow accompanied by mild strombolian activity in 2015 at the Central Crater would mark the complete emptying of the NSEC magma reservoir. Therefore, the following activity of Mt. Etna indicates a deep change in the dynamics of this volcano with the end of the predominant role of the SEC-NSEC in driving summit eruptions and the beginning of a new phase characterized by eruptions mostly at the Central Crater.

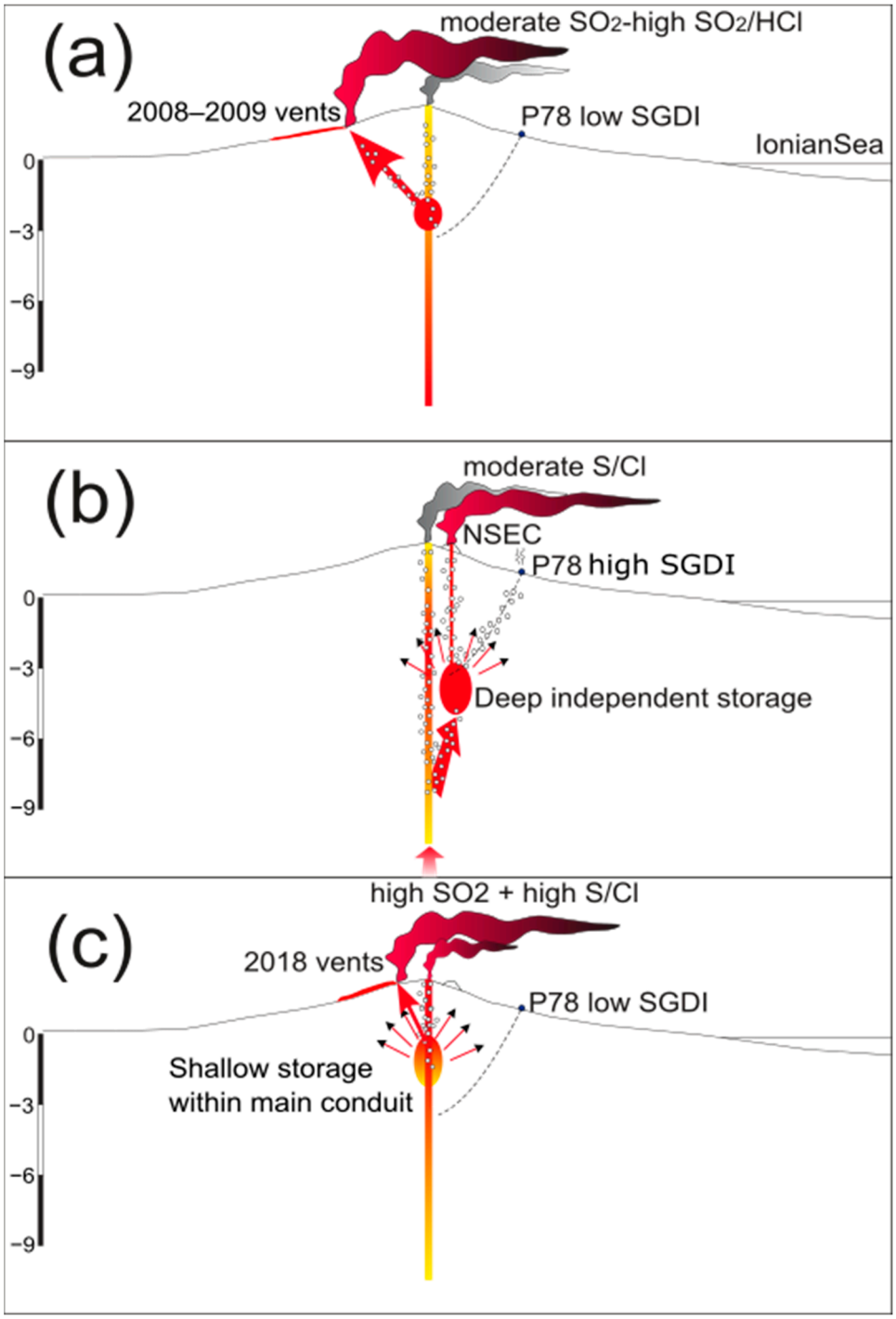

Figure 6. Schematic dynamic model that explains the behavior of crater and flank degassing at Mt. Etna associated with volcanic activity and ground deformation during the study period. (**a**) Situation as envisaged before 2009; (**b**) situation during the period 2009–2014; (**c**) situation from about 2015 to 2020. See text for details. Large red arrows indicate the main pathways of magma motion inside the volcano; small red arrows with black head indicate gas overpressure (i.e., sources of inflation) in magma reservoirs.

6. Conclusions

The combined monitoring of crater gas emissions, both in terms of their fluxes and of the molar ratios of gas species having different depth of exsolution, is highly effective in describing the dynamics of magma in the main feeding conduits of Mt. Etna. Adding

a physico-chemical parameter measured from distal emissions from the volcano flanks, such as the SGDI, allows to better constrain the gas pressure conditions within a volcanic system and to observe pressure changes related with the motion of new magma (and its velocity of migration) toward the surface. If this holds true, then the monitoring site P78 assumes a great importance in the detection of gas pressure anomalies related with storage of fresh magma into relatively shallow reservoirs that in some ways form inside faults that are connected with the structural systems of the east flank of Mt. Etna.

A higher frequency of acquisition of all considered parameters would greatly improve the amount of information to be obtained, also allowing for a more efficient filtering of the acquired signals.

Author Contributions: Conceptualization, S.G., G.S. and A.L.S.; methodology, S.G., G.S., P.B., A.L.S., T.C., S.R.M., F.M. and P.P.; formal analysis, S.G., P.B. and G.S.; data curation, S.G., G.S., A.L.S. and F.M.; writing—original draft preparation, S.G.; writing—review and editing, S.G., G.S., A.L.S. and P.B. All authors have read and agreed to the published version of the manuscript.

Funding: This research received funding from the National Institute of Geophysics and Volcanology of Italy (INGV), through its Departmental Strategic Project IMPACT.

Data Availability Statement: The data presented in this article will be made available by the corresponding author on reasonable request.

Acknowledgments: We thank F. Calvagna, S. Consoli and M. Lopez for their help in collecting the SGDI data on the field.

Conflicts of Interest: The authors declare no conflicts of interest. The funders had no role in the design of the study; in the collection, analyses, or interpretation of data; in the writing of the manuscript, or in the decision to publish the results.

References

1. Fischer, T.P.; Chiodini, G. Volcanic, Magmatic and Hydrothermal Gases. In *The Encyclopedia of Volcanoes*; Sigurdsson, H., Houghton, B., McNutt, S., Rymer, H., Stix, J., Eds.; Elsevier: London, UK, 2015; pp. 779–797.
2. Pyle, D.M.; Mather, T.A.; Biggs, J. Remote Sensing of Volcanoes and Volcanic Processes: Integrating Observation and Modelling—Introduction. *Geol. Soc. Lond. Spec. Publ.* **2013**, *380*, 1–13. [CrossRef]
3. Edmonds, M. New Geochemical Insights into Volcanic Degassing. *Philos. Trans. R. Soc. Math. Phys. Eng. Sci.* **2008**, *366*, 4559–4579. [CrossRef] [PubMed]
4. Burton, M.; Allard, P.; Muré, F.; La Spina, A. Magmatic Gas Composition Reveals the Source Depth of Slug-Driven Strombolian Explosive Activity. *Science* **2007**, *317*, 227–230. [CrossRef] [PubMed]
5. Oppenheimer, C. Volcanic Degassing. In *Treatise on Geochemistry*; Elsevier: Amsterdam, The Netherlands, 2003; pp. 123–166.
6. Moretti, R.; Métrich, N.; Arienzo, I.; Di Renzo, V.; Aiuppa, A.; Allard, P. Degassing vs. Eruptive Styles at Mt. Etna Volcano (Sicily, Italy). Part I: Volatile Stocking, Gas Fluxing, and the Shift from Low-Energy to Highly Explosive Basaltic Eruptions. *Chem. Geol.* **2018**, *482*, 1–17. [CrossRef]
7. Spilliaert, N.; Métrich, N.; Allard, P. S–Cl–F Degassing Pattern of Water-Rich Alkali Basalt: Modelling and Relationship with Eruption Styles on Mount Etna Volcano. *Earth Planet. Sci. Lett.* **2006**, *248*, 772–786. [CrossRef]
8. Delmelle, P.; Stix, J. Volcanic Gases. *Encycl. Volcanoes* **2011**, *63*, 803–815.
9. Stolper, E.; Holloway, J.R. Experimental Determination of the Solubility of Carbon Dioxide in Molten Basalt at Low Pressure. *Earth Planet. Sci. Lett.* **1988**, *87*, 397–408. [CrossRef]
10. Pan, V.; Holloway, J.R.; Hervig, R.L. The Pressure and Temperature Dependence of Carbon Dioxide Solubility in Tholeiitic Basalt Melts. *Geochim. Cosmochim. Acta* **1991**, *55*, 1587–1595. [CrossRef]
11. Clocchiatti, R.; Weisz, J.; Mosbah, M.; Tanguy, J.C. Coexistence de "Verres" Alcalins et Tholéiitiques Saturés En CO_2 Dans Les Olivines Des Hyaloclastites d'Aci Castello (Etna, Sicile, Italie). Arguments En Faveur d'un Manteau Anormal et d'un Réservoir Profond. *Acta Vulcanol.* **1992**, *2*, 161–173.
12. Carroll, M.R.; Webster, J.D. Solubilities of Sulfur, Noble Gases, Nitrogen, Chlorine and Fluorine in Magmas. In *Volatiles in Magmas*; Carroll, M.R., Holloway, J.R., Eds.; De Gruyter: Berlin, Germany, 2018; pp. 231–280. ISBN 978-1-5015-0967-4.
13. Metrich, N.; Clocchiatti, R.; Mosbah, M.; Chaussidon, M. The 1989–1990 Activity of Etna Magma Mingling and Ascent of H_2O-Cl-S-rich Basaltic Magma. Evidence from Melt Inclusions. *J. Volcanol. Geotherm. Res.* **1993**, *59*, 131–144. [CrossRef]
14. Métrich, N.; Allard, P.; Spilliaert, N.; Andronico, D.; Burton, M. 2001 Flank Eruption of the Alkali- and Volatile-Rich Primitive Basalt Responsible for Mount Etna's Evolution in the Last Three Decades. *Earth Planet. Sci. Lett.* **2004**, *228*, 1–17. [CrossRef]
15. Holloway, J.R.; Blank, J.G. Application of Experimental Results to C-O-H Species in Natural Melts. In *Volatiles in Magmas*; Carroll, M.R., Holloway, J.R., Eds.; De Gruyter: Berlin, Germany; Boston, MA, USA, 2018; Volume 30.

16. Lesne, P.; Kohn, S.C.; Blundy, J.; Witham, F.; Botcharnikov, R.E.; Behrens, H. Experimental Simulation of Closed-System Degassing in the System Basalt-H_2O-CO_2-S-Cl. *J. Petrol.* **2011**, *52*, 1737–1762. [CrossRef]
17. La Spina, A.; Burton, M.; Salerno, G.; Caltabiano, T. Insights into Magma Dynamics at Etna (Sicily) from SO_2 and HCl Fluxes during the 2008–2009 Eruption. *Geology* **2023**, *51*, 419–423. [CrossRef]
18. Giammanco, S.; Bonfanti, P. Cluster Analysis of Soil CO_2 Data from Mt. Etna (Italy) Reveals Volcanic Influences on Temporal and Spatial Patterns of Degassing. *Bull. Volcanol.* **2009**, *71*, 201–218. [CrossRef]
19. Giammanco, S.; Sims, K.W.W. Monitoring Volcanic Activity through Combined Measurements of CO_2 Efflux and (^{222}Rn) and (^{220}Rn) in Soil Gas: An Application to Mt. Etna (Italy). In *Isotopic Constraints on Earth System Processes*; Sims, K., Maher, K., Schrag, D., Eds.; Wiley: Hoboken, NJ, USA, 2022; pp. 167–202. ISBN 978-1-119-59500-7.
20. Neri, M.; Ferrera, E.; Giammanco, S.; Currenti, G.; Cirrincione, R.; Patanè, G.; Zanon, V. Soil Radon Measurements as a Potential Tracer of Tectonic and Volcanic Activity. *Sci. Rep.* **2016**, *6*, 24581. [CrossRef]
21. Caltabiano, T.; Burton, M.; Giammanco, S.; Allard, P.; Bruno, N.; Murè, F.; Romano, R. Volcanic Gas Emissions from the Summit Craters and Flanks of Mt. Etna, 1987–2000. In *Mt. Etna: Volcano Laboratory*; Bonaccorso, A., Calvari, S., Coltelli, M., Del Negro, C., Falsaperla, S., Eds.; Geophysical Monograph Series; American Geophysical Union: Washington, DC, USA, 2004; Volume 143, pp. 111–128. [CrossRef]
22. Giammanco, S.; Neri, M.; Salerno, G.G.; Caltabiano, T.; Burton, M.R.; Longo, V. Evidence for a Recent Change in the Shallow Plumbing System of Mt. Etna (Italy): Gas Geochemistry and Structural Data during 2001–2005. *J. Volcanol. Geotherm. Res.* **2013**, *251*, 90–97. [CrossRef]
23. Behncke, B.; Branca, S.; Corsaro, R.A.; De Beni, E.; Miraglia, L.; Proietti, C. The 2011–2012 Summit Activity of Mount Etna: Birth, Growth and Products of the New SE Crater. *J. Volcanol. Geotherm. Res.* **2014**, *270*, 10–21. [CrossRef]
24. De Beni, E.; Behncke, B.; Branca, S.; Nicolosi, I.; Carluccio, R.; D'Ajello Caracciolo, F.; Chiappini, M. The Continuing Story of Etna's New Southeast Crater (2012–2014): Evolution and Volume Calculations Based on Field Surveys and Aerophotogrammetry. *J. Volcanol. Geotherm. Res.* **2015**, *303*, 175–186. [CrossRef]
25. Andronico, D.; Cannata, A.; Di Grazia, G.; Ferrari, F. The 1986–2021 Paroxysmal Episodes at the Summit Craters of Mt. Etna: Insights into Volcano Dynamics and Hazard. *Earth-Sci. Rev.* **2021**, *220*, 103686. [CrossRef]
26. Calvari, S.; Salerno, G.G.; Spampinato, L.; Gouhier, M.; La Spina, A.; Pecora, E.; Harris, A.J.L.; Labazuy, P.; Biale, E.; Boschi, E. An Unloading Foam Model to Constrain Etna's 11–13 January 2011 Lava Fountaining Episode. *J. Geophys. Res. Solid Earth* **2011**, *116*, B11207. [CrossRef]
27. Salerno, G.G.; Burton, M.R.; Oppenheimer, C.; Caltabiano, T.; Randazzo, D.; Bruno, N.; Longo, V. Three-Years of SO_2 Flux Measurements of Mt. Etna Using an Automated UV Scanner Array: Comparison with Conventional Traverses and Uncertainties in Flux Retrieval. *J. Volcanol. Geotherm. Res.* **2009**, *183*, 76–83. [CrossRef]
28. Salerno, G.G.; Burton, M.R.; Oppenheimer, C.; Caltabiano, T.; Tsanev, V.I.; Bruno, N. Novel Retrieval of Volcanic SO_2 Abundance from Ultraviolet Spectra. *J. Volcanol. Geotherm. Res.* **2009**, *181*, 141–153. [CrossRef]
29. Sellitto, P.; Salerno, G.; La Spina, A.; Caltabiano, T.; Terray, L.; Gauthier, P.J.; Briole, P. A Novel Methodology to Determine Volcanic Aerosols Optical Properties in the UV and NIR and Ångström Parameters Using Sun Photometry. *J. Geophys. Res. Atmos.* **2017**, *122*, 9803–9815. [CrossRef]
30. Francis, P.; Burton, M.R.; Oppenheimer, C. Remote Measurements of Volcanic Gas Compositions by Solar Occultation Spectroscopy. *Nature* **1998**, *396*, 567–570. [CrossRef]
31. Cardellini, C.; Chiodini, G.; Frondini, F. Application of Stochastic Simulation to CO_2 Flux from Soil: Mapping and Quantification of Gas Release. *J. Geophys. Res. Solid Earth* **2003**, *108*, 3-1–3-13. [CrossRef]
32. Chiodini, G.; Cioni, R.; Guidi, M.; Raco, B.; Marini, L. Soil CO_2 Flux Measurements in Volcanic and Geothermal Areas. *Appl. Geochem.* **1998**, *13*, 543–552. [CrossRef]
33. Klusman, R.W. Comparison of Surface and Near-Surface Geochemical Methods for Detection of Gas Microseepage from Carbon Dioxide Sequestration. *Int. J. Greenh. Gas Control* **2011**, *5*, 1369–1392. [CrossRef]
34. Lane-Smith, D.; Sims, K.W.W. The Effect of CO_2 on the Measurement of ^{220}Rn and ^{222}Rn with Instruments Utilising Electrostatic Precipitation. *Acta Geophys.* **2013**, *61*, 822–830. [CrossRef]
35. Aiuppa, A.; Allard, P.; D'Alessandro, W.; Giammanco, S.; Parello, F.; Valenza, M. Magmatic Gas Leakage at Mount Etna (Sicily, Italy): Relationships with the Volcano-Tectonic Structures, the Hydrological Pattern and the Eruptive Activity. In *Mt. Etna: Volcano Laboratory*; Bonaccorso, A., Calvari, S., Coltelli, M., Del Negro, C., Falsaperla, S., Eds.; Geophysical Monograph Series; American Geophysical Union: Washington, DC, USA, 2004; Volume 143, pp. 129–145. [CrossRef]
36. Giammanco, S.; Inguaggiato, S.; Valenza, M. Soil and Fumarole Gases of Mount Etna: Geochemistry and Relations with Volcanic Activity. *J. Volcanol. Geotherm. Res.* **1998**, *81*, 297–310. [CrossRef]
37. Johnová, K.; Thinová, L.; Giammanco, S. Revealing the Hidden Faults in the SE Flank of Mt. Etna Using Radon in-Soil Gas Measurement. *Radiat. Prot. Dosim.* **2014**, *160*, 70–73. [CrossRef]
38. Bonaccorso, A.; Aloisi, M. Tracking Magma Storage: New Perspectives From 40 Years (1980–2020) of Ground Deformation Source Modeling on Etna Volcano. *Front. Earth Sci.* **2021**, *9*, 638742. [CrossRef]
39. Firetto Carlino, M.; Scarfì, L.; Cannavò, F.; Barberi, G.; Patanè, D.; Coltelli, M. Frequency-Magnitude Distribution of Earthquakes at Etna Volcano Unravels Critical Stress Changes along Magma Pathways. *Commun. Earth Environ.* **2022**, *3*, 68. [CrossRef]

40. Granieri, D.; Chiodini, G.; Marzocchi, W.; Avino, R. Continuous Monitoring of CO_2 Soil Diffuse Degassing at Phlegraean Fields (Italy): Influence of Environmental and Volcanic Parameters. *Earth Planet. Sci. Lett.* **2003**, *212*, 167–179. [CrossRef]
41. Hinkle, M.E. Environmental Conditions Affecting Concentrations of He, CO_2, O_2 and N_2 in Soil Gases. *Appl. Geochem.* **1994**, *9*, 53–63. [CrossRef]
42. King, C.Y. Episodic Radon Changes in Subsurface Soil Gas along Active Faults and Possible Relation to Earthquakes. *J. Geophys. Res.* **1980**, *85*, 3065–3078. [CrossRef]
43. Klusman, R.W.; Jaacks, J.A. Environmental Influences upon Mercury, Radon and Helium Concentrations in Soil Gases at a Site near Denver, Colorado. *J. Geochem. Explor.* **1987**, *27*, 259–280. [CrossRef]
44. Pérez, N.M.; Hernández, P.A.; Padrón, E.; Cartagena, R.; Olmos, R.; Barahona, F.; Melián, G.; Salazar, P.; López, D.L. Anomalous Diffuse CO_2 Emission Prior to the January 2002 Short-Term Unrest at San Miguel Volcano, El Salvador, Central America. *Pure Appl. Geophys.* **2006**, *163*, 883–896. [CrossRef]
45. Rogie, J.D.; Kerrick, D.M.; Sorey, M.L.; Chiodini, G.; Galloway, D.L. Dynamics of Carbon Dioxide Emission at Mammoth Mountain, California. *Earth Planet. Sci. Lett.* **2001**, *188*, 535–541. [CrossRef]
46. Salazar, J.M.L.; Pérez, N.M.; Hernández, P.A.; Soriano, T.; Barahona, F.; Olmos, R.; Cartagena, R.; López, D.L.; Lima, R.N.; Melián, G.; et al. Precursory Diffuse Carbon Dioxide Degassing Signature Related to a 5.1 Magnitude Earthquake in El Salvador, Central America. *Earth Planet. Sci. Lett.* **2002**, *205*, 81–89. [CrossRef]
47. Sugisaki, R.; Ido, M.; Takeda, H.; Isobe, Y.; Hayashi, Y.; Nakamura, N.; Satake, H.; Mizutani, Y. Origin of Hydrogen and Carbon Dioxide in Fault Gases and Its Relation to Fault Activity. *J. Geol.* **1983**, *91*, 239–258. [CrossRef]
48. Thomas, D.M.; Cotter, J.M.; Holford, D. Experimental Design for Soil Gas Radon Monitoring. *J. Radioanal. Nucl. Chem.* **1992**, *161*, 313–323. [CrossRef]
49. Barnet, I.; Procházka, J.; Skalský, L. Do the Earth Tides Have an Influence on Short-Term Variations in Radon Concentration? *Radiat. Prot. Dosim.* **1997**, *69*, 51–60. [CrossRef]
50. Cigolini, C.; Poggi, P.; Ripepe, M.; Laiolo, M.; Ciamberlini, C.; Delle Donne, D.; Ulivieri, G.; Coppola, D.; Lacanna, G.; Marchetti, E.; et al. Radon Surveys and Real-Time Monitoring at Stromboli Volcano: Influence of Soil Temperature, Atmospheric Pressure and Tidal Forces on 222Rn Degassing. *J. Volcanol. Geotherm. Res.* **2009**, *184*, 381–388. [CrossRef]
51. Koike, K.; Yoshinaga, T.; Asaue, H. Characterizing Long-Term Radon Concentration Changes in a Geothermal Area for Correlation with Volcanic Earthquakes and Reservoir Temperatures: A Case Study from Mt. Aso, Southwestern Japan. *J. Volcanol. Geotherm. Res.* **2014**, *275*, 85–102. [CrossRef]
52. Kraner, H.; Schroeder, G.; RD, E. Measurements of the Effects of Atmospheric Variables on Radon-222 Flux and Soil Gas Concentrations. In *The Natural Radiation Environment*; Adams, J.A., Lowder, W.M., Eds.; University of Chicago Press: Chicago, IL, USA, 1964; pp. 191–215.
53. Schumann, R.R.; Owen, D.E. *Relationships between Geology, Equivalent Uranium Concentration, and Radon in Soil Gas*; USGS Open File Report 88-18; U.S. Geological Survey: Reston, VA, USA, 1988; pp. 1–28. [CrossRef]
54. İçhedef, M.; Giammanco, S.; Neri, M.; Catalano, R.; Immé, G.; Morelli, D.; Muré, F.; Giudice, N. In Soil Radon Anomalies and Volcanic Activity on Mt. Etna (Italy). *J. Environ. Radioact.* **2020**, *218*, 106267. [CrossRef]
55. Mattia, M.; Bruno, V.; Montgomery-Brown, E.; Patanè, D.; Barberi, G.; Coltelli, M. Combined Seismic and Geodetic Analysis Before, During, and After the 2018 Mount Etna Eruption. *Geochem. Geophys. Geosyst.* **2020**, *21*, e2020GC009218. [CrossRef]
56. La Spina, A.; Salerno, G. *Composizione del Gas Emesso dalla Bocca Apertasi Il 6 Novembre 2009 alla Base del Cratere di Sud-Est*; Internal Protocol UFVG2009/88 Internal Report; Istituto Nazionale di Geofisica e Vulcanologia: Rome, Italy, 2009; 3p.
57. Liuzzo, M.; Gurrieri, S.; Giudice, G.; Giuffrida, G. Ten Years of Soil CO_2 Continuous Monitoring on Mt. Etna: Exploring the Relationship between Processes of Soil Degassing and Volcanic Activity. *Geochem. Geophys. Geosyst.* **2013**, *14*, 2886–2899. [CrossRef]